Scripta Materialia 248 (2024) 116127

Contents lists available at ScienceDirect

Scripta Materialia

journal homepage: www.journals.elsevier.com/scripta-materialia

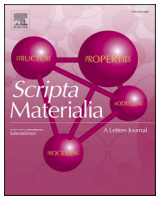

On the fcc to hcp transformation in a Co-Ru alloy: Variant selection and intervariant boundary character☆

E. Farabi [a,*], N. Haghdadi [a], C. Czettl [b], J. Pachlhofer [b], G.S. Rohrer [c], S.P. Ringer [d], S. Primig [a,*]

[a] School of Materials Science & Engineering, UNSW Sydney, NSW 2052, Australia
[b] R&D Carbide and Coating, CERATIZIT Austria GmbH, Metallwerk-Plansee-Straße 71, Reutte 6600, Austria
[c] Department of Materials Science and Engineering, Carnegie Mellon University, Pittsburgh, PA 15213-3890, USA
[d] Australian Centre for Microscopy and Microanalysis and School of Aerospace, Mechanical & Mechatronic Engineering, The University of Sydney, NSW 2006, Australia

ARTICLE INFO

Keywords:
Co-binder alloys
Martensite
Crystallographic analysis
Variant selection
Habit plane

ABSTRACT

Ru is a common addition to the Co-binder in WC—Co hardmetals for advanced cutting tool applications. Internal Co-Co interfaces control many properties such as hot-hardness, toughness, and creep resistance. Hence, phase transformations determining the internal interface character can be harnessed to achieve superior properties. We investigate the γ (face-centred cubic) to α (hexagonally closed packed) martensitic phase transformation of a model Co-Ru binder alloy. We describe the crystallography of γ to α phase transformations and the resulting α/γ and α/α interface character distributions. The stabilisation of the γ-phase results in the formation of low energy (0 0 0 1) α/γ interphase boundary planes. Preferred formation of α/α intervariant and twin-related boundaries with symmetrical tilt configurations are also observed. We discuss how crystallographic constraints of the transformation promote the formation of grain boundary planes other than those of the lowest energy configurations.

Co is commonly used as a binder for WC particles in WC—Co hardmetals for advanced cutting tool applications such as precision CNC machining inserts. WC—Co materials offer remarkable mechanical properties such as excellent resistance to wear, high temperature strength, and sufficient toughness [1,2]. Several critical mechanical and technological properties of WC—Co hardmetals are controlled by internal Co-Co interfaces in the Co-binder which has two allotropic phases, a low-temperature hexagonally-closed packed (hcp) α-phase and a high-temperature face-centred cubic (fcc) γ-phase [3]. The Co-binder is a solid solution, containing small amounts of C and W dissolved during the sintering process [4,5]. In addition, alloying elements such as Ru [6,7], Rh [8] and/or *Re* [9,10] are added to the Co-binder to improve hot-hardness, toughness, and creep resistance of WC—Co hardmetals. This affects the stability ranges of the constituent phases, stacking fault energy (SFE) and thus, deformation mechanisms of the Co-binder alloy [11,12]. It is known that twin platelets and transformation-induced interfaces provide intragranular barriers to slip in the Co-binder which determines the in-service performance of WC—Co [12–14]. This opens new opportunities to optimise the properties of WC—Co hardmetals by controlling the phase stability and resultant interface network of the Co-binder.

Phase transformations are an effective way to engineer the interface character and grain boundary network of crystalline materials [15,16]. In Co-alloys, the fcc (γ) ↔ hcp (α) phase transformations follows the Shoji-Nishiyama orientation relationship (S-N OR), where one of the close-packed $\{1\ 1\ 1\}_\gamma$ planes in the γ-phase transforms into the basal plane of the α-phase [1,17]. This is commenced by shear on each close-packed plane by $1/6\langle 1\ 1\ \bar{2}\ 0\rangle_\alpha$ type Shockley partials, resulting a $(1\ 1\ 1)_\gamma \rightarrow (0\ 0\ 0\ 1)_\alpha$, $[1\ \bar{1}\ 0]_\gamma \rightarrow [1\ 1\ \bar{2}\ 0]_\alpha$ lattice correspondence. According to S-N OR, a single γ-grain can transform into four distinct orientations (variants), that are connected by twin-related $70.5°/\langle 1\ 1\ \bar{2}\ 0\rangle_\alpha$ rotations [14,18]. In addition, following the theoretical calculations and experimental observations from Yang and Wayman [19,20], new hcp variants at the intersection of the primary variants can be formed during the fcc ↔ hcp phase transformation. These new variants form due to intersecting homogeneous shear of the primary hcp variants, distorting the intersected region into a new fcc

☆ G.S. Rohrer was an Editor of the journal during the review period of the article. To avoid a conflict of interest, G.S. Rohrer was blinded to the record and another editor processed this manuscript.

* Corresponding authors.
E-mail addresses: e.farabi@unsw.edu.au (E. Farabi), s.primig@unsw.edu.au (S. Primig).

https://doi.org/10.1016/j.scriptamat.2024.116127
Received 23 January 2024; Received in revised form 20 March 2024; Accepted 11 April 2024
Available online 20 April 2024

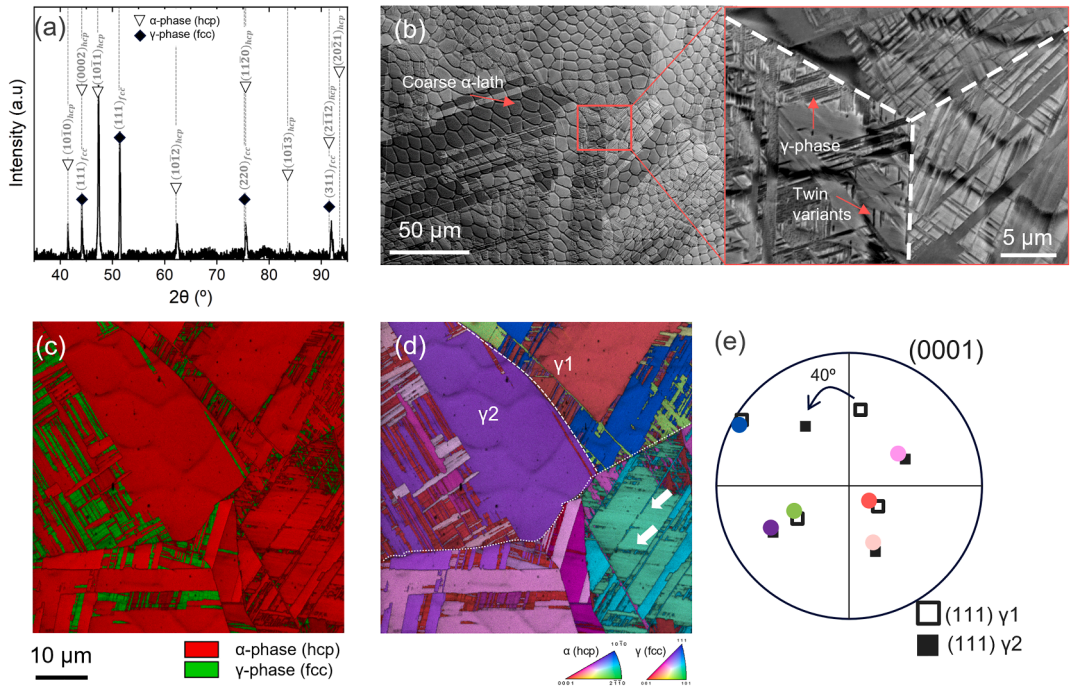

Fig. 1. (a) XRD pattern, (b) backscattered SEM image with cellular structure from casting, (c) phase map, and (d) inverse pole figure map of the Co11Ru alloy. (e) (0 0 0 1)$_\alpha$ pole figure projection of α-variants and superimposed (1 1 1)$_\gamma$ pole figure projections of parent grains of γ1 and γ2 in (d). The colour of the circles corresponds to the IPF colour codes of all α-variants in γ1 and γ2 in (d). The white dashed lines in (d) mark the parent γ grains.

variant which then transforms into new hcp variants (i.e., secondary hcp variants). The intersection of the primary variants with the secondary variants tend to result in interfaces with rotation angles of 19.5, 31.5, 39, 51 and 90° about a common $<1\ 1\ \bar{2}\ 0>_\alpha$ axis or multiple irrational rotations [19,20].

The crystallography and kinetics of hcp ↔ fcc phase transformations have been researched over the past decades [17,19–21]. There are reports on the morphology [22,23], orientation relationship [17,24], habit planes [20,25], dislocation substructures of laths and grains [26,27], and the impact of twinning [28,29]. Some efforts were made to characterise the crystallography of interfaces using transmission electron microscopy (TEM), however, this has so far been limited to 2D characteristics of a small number of α/α interfaces [14,28,30]. The crystallography, energy, and network of the possible interphase/boundaries in Co-binder alloys remain unknown. In the past, it was too challenging to measure all five independent crystallographic parameters due to time limits and the complexity of experiments or computations. However, recent advancements in automated microscopy have enabled the measurement of the grain boundary character distribution (GBCD) and the relative energetic characteristics for a range of materials. Given the martensitic transformation of the Co-binder during manufacturing of hardmetals, a better understanding of the evolution of its interfaces is crucial, as control of the interface character can be harnessed to achieve superior properties. However, knowledge of the crystallographic nature of the martensitic phase transformation in the Co-Ru system and the resulting α/γ and α/α interface character distributions remains limited.

Hence, we here systematically investigate the γ to α martensitic phase transformation in Co-Ru binders that are used for milling Ni-based and Ti-alloys in particular. We apply statistical stereology on interface traces from 2D electron back-scatter diffraction (EBSD) to identify the plane distributions and various interface characteristics [31,32]. We mainly focus on primary variants formed via a S-N OR and extension twins in the as-cast condition. Although this method has been used to characterise the distribution of grain boundaries formed during the fcc ↔ body-centred cubic (bcc) and bcc ↔ hcp phase transformations in steels and Ti-6Al-4V [33,34], there is currently no reported research offering a fundamental characterisation and a statistical overview of interfaces forming during the fcc → hcp phase transformation.

The Co-Ru phase diagram in Supplementary Fig. S1 was predicted using the Thermo-Calc 2021b software and the TCHEA5 database for high entropy alloys. The γ- and α-phase fractions of the equilibrium state of several Co-Ru compositions were determined at 700 °C. A Co-11 wt.% Ru model alloy (referred to as Co11Ru hereafter) was selected to achieve a suitable fraction of γ-phase in its as-cast state (i.e., 13.9 %). Pure Co (99.9999 %) was alloyed with 11 wt.% Ru (99.9999 %) and cast using an Edmund Bühler Mini Arc Melter MAM-1 in an Ar atmosphere. The constituent phases of the casting were identified on a PANalytical X-ray diffractometer (XRD) equipped with a Cu-Kα source, using a point scan with a 0.015° step size and 8 s dwell time. The background of the XRD data is subtracted by the automatic background removal function of the WINPLOTR software embedded into the FullProf suite (Version 2.00). Multiple samples were polished to a 0.05 μm oxide polishing suspension finish for microstructure characterisation. EBSD maps were collected in a JEOL 7001 scanning electron microscope (SEM) equipped with a Hikari 31 EBSD camera. Further parameters are an accelerating voltage of 20 kV, working distance of 12 mm, step size of 50 nm, and 4 × 4 binning. Multiple 65 × 65 μm^2 maps from two perpendicular cross sections were obtained to minimise the effects of texture and grain morphology. The collected data was processed using TSL software V8.0. Before extracting interfaces, several clean-up procedures, as described in [35], were applied.

The XRD results and back scattered SEM images of the as-cast Co11Ru alloy in Fig. 1a, b show both α- and γ-phases, suggesting that the high-temperature γ-phase did not fully transform to α-phase. The overall microstructure shows cellular characteristics expected from the as-cast conditions. During the phase transformation, the pre-existing γ-grain boundaries serve as primary sites for α-lath martensite nucleation, as depicted in Fig. 1b (white dashed lines). Notably, it is observed that the α-laths tend to nucleate with distinct orientations on opposite sides of individual γ-grain boundaries (Fig. 1b–d). Two lath morphologies are frequently detected including elongated coarse martensitic laths that span across the entire parent γ-grains and that are stacked into

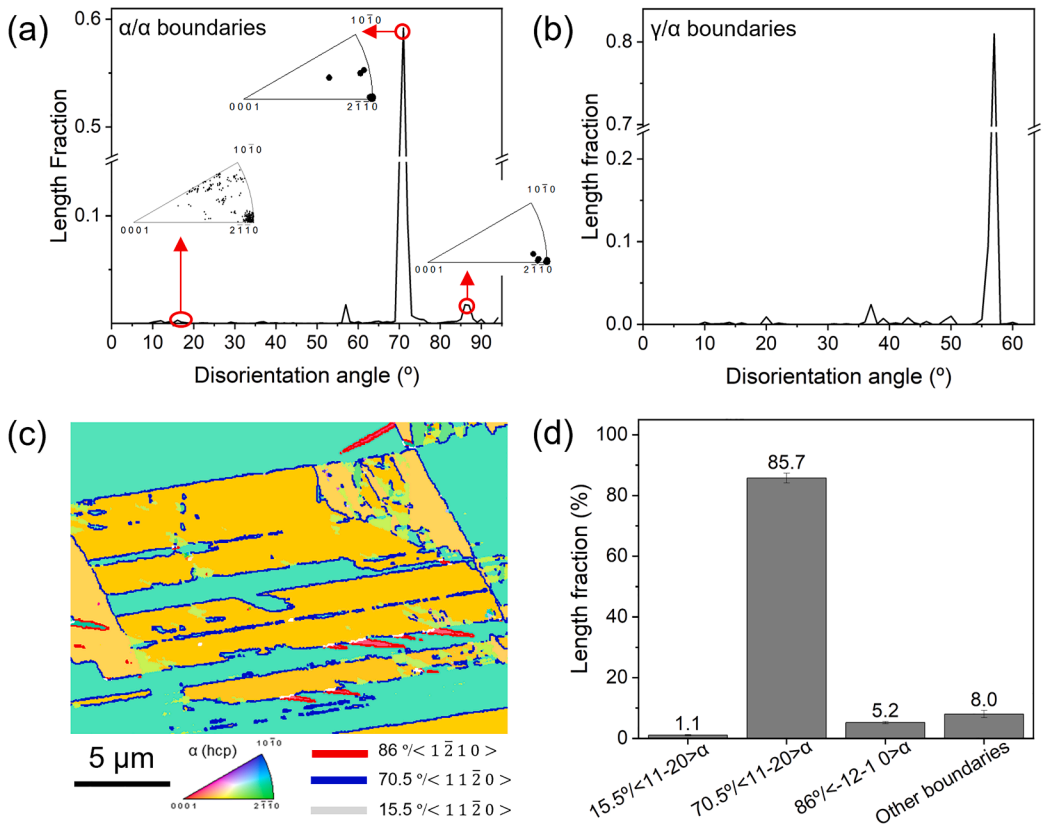

Fig. 2. Disorientation angle distributions for (a) α/α and (b) γ/α boundaries. (c) A representative boundary map illustrating major hcp/hcp characteristic boundaries and, (d) distribution of hcp/hcp intervariant boundaries associated with the S-N OR. The insets in (a) show axes distributions corresponding to different disorientation angle peaks.

parallel or intersecting arrays (Figs. 1b and S2). These laths are largely separated by either low angle or high angle boundaries (Fig. S2a). The second morphology consists of fine lath-like structures formed inside the coarser laths largely separated by twin related boundaries (86°/$<\bar{1}\ 2\ \bar{1}\ 0>_{\alpha}$ extension twins, Fig. S2b). The inverse pole figure map reveals these twins as fine parallel lines within selected primary coarse laths (as depicted by the white arrow in Figs. 1d and S2b). Microscopic shear in martensitic transformations is accommodated by Shockley partials [21,36]. Consequently, these twins are not transformation products but can be attributed to solidification-induced internal stresses such as volumetric shrinkage and thermal stresses [37].

The pole figures corresponding to the two prior γ-grains and the transformed α laths are provided in Fig. 1e. It is apparent that high-temperature γ-grains are transformed into multiple α-variants and share a common $(0\ 0\ 0\ 1)_{\alpha}$ pole with the $(1\ 1\ 1)_{\gamma}$ poles of the parent γ-grains. Variants can be related through a 70.5° rotation of the basal

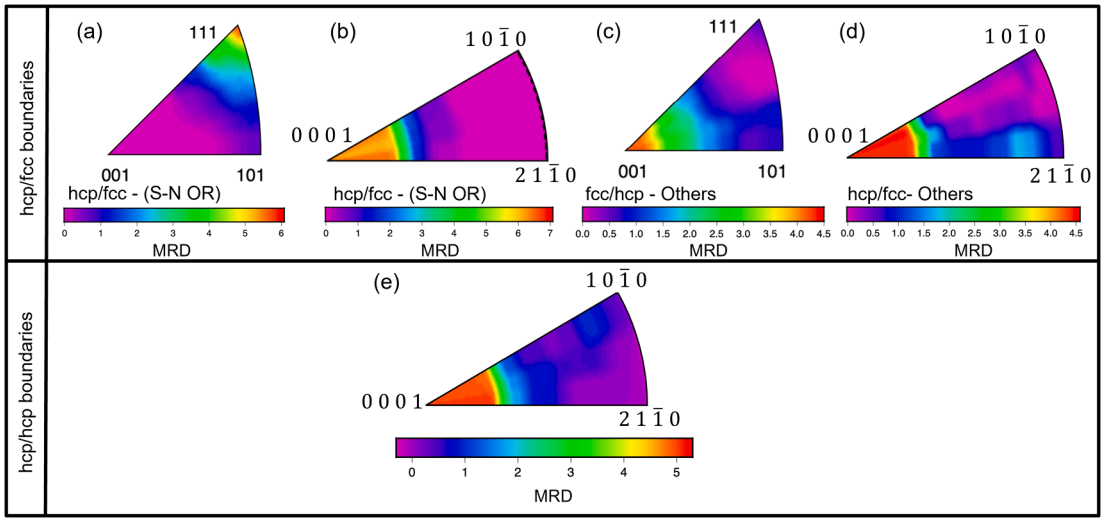

Fig. 3. Distributions of the hcp-fcc interface boundary planes following the S-N OR (i.e., 56.6°/<76 $\overline{59}$ 24>) presented in (a) an fcc lattice frame and (b) an hcp lattice frame. Interfaces not following the S-N OR are presented in (c) an fcc lattice frame and (d) an hcp lattice frame. (e) Distribution of hcp/hcp habit planes for all disorientations in the transformed microstructure. MRD stands for multiples of a random distribution.

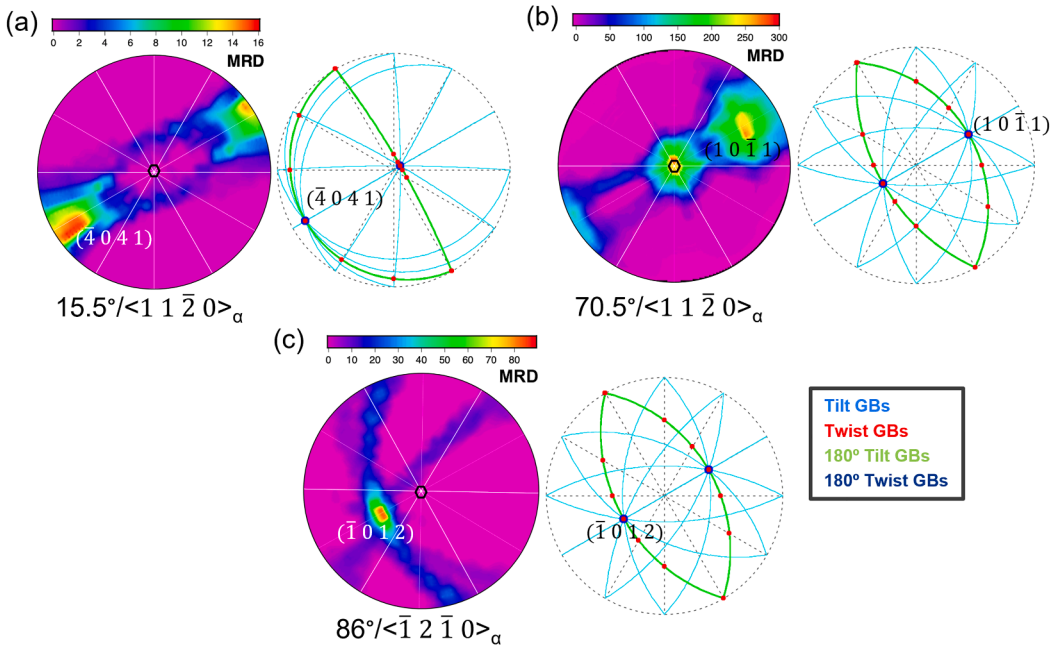

Fig. 4. α/α grain boundary character distribution at fixed disorientations of (a) 15.5°/<1 1 $\bar{2}$ 0>$_\alpha$, (b) 70.5°/<1 1 $\bar{2}$ 0>$_\alpha$, (c) 86°/<$\bar{1}$ 2 $\bar{1}$ 0>$_\alpha$, and corresponding theoretical characteristic boundaries using Glowinski's grain boundary toolbox software [41]. The hexagon in the centre of the stereographs represents the (0 0 0 1) orientation. MRD denotes multiples of random distribution.

plane around the <0 1 1>$_\gamma$ direction (zone axis) [17,20]. Therefore, it is expected that the transformed α-variants are separated by 70.5°/<1 1 $\bar{2}$ 0>$_\alpha$ intervariant boundaries. In contrast to previous reports [18,38], no twin relationship (Σ3 boundaries) between prior γ-grains is observed here (Fig. 1e).

The α/α disorientation angle distribution shows the expected pronounced peak at ~70.5° and smaller peaks at around 15–20°, 55–60°, and 85–90° (Fig. 2a). On the other hand, the disorientation angle distribution of α/γ boundaries exhibits a distinct peak at around 54–58° (Fig. 2b). This peak aligns well with the anticipated disorientation angles and axes inherent to the S-N OR, defined by 56.6° rotations around <77 $\overline{59}$ 24> [39]. As for the α/α boundaries, the corresponding axis for 70.5° is <1 1 $\bar{2}$ 0>$_\alpha$ (i.e., the S-N OR), while the 15–20° and 85–90° peaks correlate to the rational <1 1 $\bar{2}$ 0>$_\alpha$ and <$\bar{1}$ 2 $\bar{1}$ 0>$_\alpha$ axes, respectively. This means that the peak around 85–90° can be related to the 86°/<$\bar{1}$ 2 $\bar{1}$ 0>$_\alpha$ extension twin relationship [27].

The observed 15–20° peaks can be related to the intersection of a primary variant (70.5°/<1 1 $\bar{2}$ 0>$_\alpha$) with an extension twin variant 86°/<$\bar{1}$ 2 $\bar{1}$ 0>$_\alpha$ resulting in a rotation of 86°- 70.5° = 15.5° around <1 1 $\bar{2}$ 0>$_\alpha$. It may be argued that these peaks can be associated with secondary 19.5° intervariants as reported by Yang and Wayman [1,2]. However, a closer look into the intersecting variants (Fig. 2c) confirms that the peaks are mainly formed at intersecting primary α and extension twin variants. The observation of smaller peaks in the misorientation angle distribution is generally associated with intersecting variants of adjacent γ grains resulting in boundaries not related to the S-N OR (other boundaries).

The total population fraction of primary intervariants, twins and the intersecting boundaries is illustrated in Fig. 2d. The highest population is attributed to the 70.5°/<1 1 $\bar{2}$ 0>$_\alpha$ boundaries. The extension twin boundaries have a total population of 5 %. The observed 15.5°/<1 1 $\bar{2}$ 0>$_\alpha$ boundary related to intersecting twin and primary variants have the lowest total populations of 1.1 %. It should be noted that the second highest population is associated with boundaries that do not correspond to the S-N OR or twin related boundaries.

The distribution of α/γ habit planes in the fcc and hcp crystal reference frames is further investigated by plotting the relative area distributions of boundary planes in stereographic projections, irrespective of their disorientations (Fig. 3). For the boundaries following the S-N OR, the α/γ interfaces have a sharp peak at (1 1 1)$_\gamma$ within the fcc reference frame while terminating on (0 0 0 1)$_\alpha$ in hcp reference frame (Fig. 3a, b). However, for the disorientation angles following other ORs, interfaces terminate on (0 0 1)$_\gamma$ and (0 0 0 1)$_\alpha$ (Fig. 3c, d). The (0 0 0 1)$_\alpha$ and (1 1 1)$_\gamma$ planes are well known to be energetically favoured planes in hcp and fcc systems, respectively [15,34]. Furthermore, these planes closely align with predictions derived from the principles of near-coincidence site geometrical matching between hcp and fcc lattices [40].

The plane character distributions for all α/α boundaries, irrespective of disorientation angle/axes, are illustrated in Fig. 3e. The α-intervariants peak at the (0 0 0 1)$_\alpha$ position with an intensity of ~5 multiples of a random distribution (MRD). Considering the disorientation angles and axes in Fig. 2, five boundary parameters can be defined and correlated to the plane character distribution for all α/α grain boundaries (Fig. 4). The schematic representation of characteristic interfaces is developed by Glowinski's grain boundary toolbox [41]. The distribution of 15.5°/<1 1 $\bar{2}$ 0>$_\alpha$ boundaries has a maximum around ($\bar{4}$ 0 4 1), nearly an ideal symmetric tilt character (Fig. 4a). These boundaries are proper and improper quasi-symmetric character (both 180°-twist and 180°-tilt). Instead, primary 70.5°/<1 1 $\bar{2}$ 0>$_\alpha$ intervariant boundaries have a diffuse peak along prismatic (1 0 $\bar{1}$ 1)$_\alpha$ and (0 0 0 1)$_\alpha$ planes (Fig. 4b). The (0 0 0 1)$_\alpha$ boundaries have a tilt character with ~300 MRD. The (1 0 $\bar{1}$ 1)$_\alpha$ planes have a symmetric tilt character with ~250 MRD. The high intensity near (0 0 0 1)$_\alpha$ orientations confirms the predominance of basal planes in the α/α plane distribution in Fig. 3e. The (0 0 0 1)$_\alpha$ orientations are low indexed planes and energetically favoured for hcp/hcp intersections [42,43]. Finally, the boundary plane distribution for the 86°/<$\bar{1}$ 2 $\bar{1}$ 0>$_\alpha$ extension twin boundary shows a habit plane around ($\bar{1}$ 0 1 2)$_\alpha$ with an intensity of ~85 MRD (Fig. 4c). This is a symmetrical tilt boundary, showing proper and improper quasi symmetric character.

In general, an inverse correlation between the relative populations and energies of interfaces/grain boundaries is expected, as demonstrated in simulations [44,45] and experiments [46]. There is limited

Table 1
Interplanar spacings (d_{hkl}) measured for various intervariant planes and their respective population distributions.

α/α boundary	Plane	Intensity (MRD)	Interplanar spacing (Å)
15.5°/<1 1 $\bar{2}$ 0>$_\alpha$	($\bar{4}$ 0 4 1)$_\alpha$	16	0.18 or 0.36
70.5°/<1 1 $\bar{2}$ 0>$_\alpha$	(1 0 $\bar{1}$ 1)$_\alpha$	250	0.31 or 1.59
	(0 0 0 1)$_\alpha$	300	4.06
86°/<$\bar{1}$ 2 $\bar{1}$ 0>$_\alpha$	($\bar{1}$ 0 1 2)$_\alpha$	85	0.75
All boundaries	(0 0 0 1)$_\alpha$	5.5	4.06

knowledge available on the grain boundary energy in Co and its alloys. Hence, the interplanar spacing, an important criterion for assessing grain boundary energy, is studied (Table 1). Flat and smooth surfaces exhibit minimal bond breakage and maximised interplanar spacings, resulting in lower surface energies and the formation of grain boundaries with correspondingly lower energies [47,48]. It is possible to establish an inverse correlation between the grain boundary energy and the interplanar spacing [43]. For Co alloys, the basal (0 0 0 1)$_\alpha$ plane exhibits the highest interplanar spacing, measuring 4.061 Å, followed by the pyramidal planes (1 0 $\bar{1}$ 1)$_\alpha$, ($\bar{1}$ 0 1 2)$_\alpha$ and ($\bar{4}$ 0 4 1)$_\alpha$ planes with 1.59, 0.75, and 0.35 Å, respectively (see Table 1).

The distribution of α/α boundary planes is predominantly characterised by low energy basal orientations, while a smaller population is observed for pyramidal and prismatic planes (Fig. 3e). The higher energy pyramidal orientations are predominant in extension twin and intersecting variant-twin boundaries (Fig. 4). This suggests that the crystallographic constraints introduced by the martensitic transformation following the S-N OR promotes boundary planes that may not inherently exhibit low-energy configurations, as previously noted in lath martensitic steels [15,49,50] and Ti-alloys [34,51]. Higher populations of low-energy interfaces such as twin-related planes and interphase boundaries can provide barriers, sources, and storage sites for defects, and control the deformation and fracture behaviour [14,52]. Our findings can be harnessed to control the interface/boundary plane network for controlling mechanical properties of WC—Co hardmetals and Co-based alloys.

In summary, the characteristics of interfaces formed during the fcc → hcp phase transformation were studied in a model Co11wt.%Ru alloy. The α/γ interphase boundaries, following the disorientation expected from the S-N OR, are shown to exhibit high populations of low energy (0 0 0 1)$_\alpha$ and (1 1 1)$_\gamma$ interfaces. The most highly populated 70.5°/<1 1 $\bar{2}$ 0>$_\alpha$ primary α/α intervariant boundaries terminate on low energy tilt (0 0 0 1)$_\alpha$ and high energy symmetrical tilt (1 0 $\bar{1}$ 1)$_\alpha$ planes. Instead, α/α boundaries associated with extension twins and their intersection with primary variants mainly terminate on high-energy pyramidal planes with tilt and symmetrical tilt character. This suggests that the intervariant boundary planes formed by the martensitic transformation following the S-N OR are governed by crystallographic constraints rather than low-energy interface configurations. Considering the role of the binder phase interfaces on properties such as toughness and wear properties of WC—Co alloy, the obtained results pave the way towards engineering the characteristic interfaces to achieve superior properties including hot-hardness, toughness, and creep resistance.

CRediT authorship contribution statement

E. Farabi: Conceptualization, Data curation, Formal analysis, Investigation, Methodology, Validation, Visualization, Writing – original draft. **N. Haghdadi:** Data curation, Formal analysis, Investigation, Methodology, Writing – review & editing. **C. Czettl:** Resources, Writing – review & editing. **J. Pachlhofer:** Resources, Writing – review & editing. **G.S. Rohrer:** Data curation, Formal analysis, Methodology, Software, Validation, Visualization, Writing – review & editing. **S.P. Ringer:** Funding acquisition, Project administration, Resources, Writing – review & editing. **S. Primig:** Funding acquisition, Project administration, Resources, Supervision, Writing – review & editing.

Declaration of competing interest

The authors declare that they have no known competing financial interests or personal relationships that could have appeared to influence the work reported in this paper.

The author Gregory S. Rohrer is Coordinating Editor for Scripta Materialia and was not involved in the editorial review or the decision to publish this article.

Acknowledgements

The authors acknowledge funding from the Australian Research Council Linkage program (LP190100850). The authors acknowledge the facilities, scientific, and technical support provided at the Electron Microscope Unit, UNSW Sydney (Mark Wainwright Analytical Centre), a node of Microscopy Australia, a national research facility supported under the Commonwealth NCRIS program. Dr David Miskovic's help with the vacuum arc melter is gratefully acknowledged.

Supplementary materials

Supplementary material associated with this article can be found, in the online version, at doi:10.1016/j.scriptamat.2024.116127.

References

[1] W. Betteridge, Cobalt and its alloys, E. Horwood, 1982. https://books.google.com.au/books?id=Ri3hAAAACAAJ.
[2] A. Chychko, J. García, V. Collado Ciprés, E. Holmström, A. Blomqvist, HV-KIC property charts of cemented carbides: a comprehensive data collection, Int. J. Refract. Met. Hard Mater. 103 (2022) 105763, https://doi.org/10.1016/j.ijrmhm.2021.105763.
[3] D.A. Young, Phase Diagrams of the Elements, University of California Press, 2023.
[4] J.M. Marshall, M. Giraudel, The role of tungsten in the Co binder: effects on WC grain size and hcp-fcc Co in the binder phase, Int. J. Refract. Met. Hard Mater. 49 (2015) 57–66, https://doi.org/10.1016/j.ijrmhm.2014.09.028.
[5] B. Roebuck, E.A. Almond, A.M. Cottenden, The influence of composition, phase transformation and varying the relative F.C.C. and H.C.P. phase contents on the properties of dilute CoWC alloys, Mater. Sci. Eng. 66 (1984) 179–194, https://doi.org/10.1016/0025-5416(84)90179-4.
[6] L. Chipise, P.K. Jain, L.A. Cornish, Sliding wear characteristics of WC-VC-Co alloys with various Ru additions, Int. J. Refract. Met. Hard Mater. 95 (2021) 105429, https://doi.org/10.1016/j.ijrmhm.2020.105429.
[7] L. Chipise, P.K. Jain, L.A. Cornish, Influence of Ru on the hardness and fracture toughness of WC-VC-Co alloys, Int. J. Refract. Met. Hard Mater. 77 (2018) 54–60, https://doi.org/10.1016/j.ijrmhm.2018.07.008.
[8] C. Zhao, H. Lu, H. Wang, F. Tang, H. Nie, C. Hou, X. Liu, X. Song, Z. Nie, Solid-solution hardening of WC by rhenium, J. Eur. Ceram. Soc. 40 (2020) 333–340, https://doi.org/10.1016/j.jeurceramsoc.2019.09.050.
[9] K. Jing, Z. Guo, T. Hua, J. Xiong, J. Liao, L. Liang, S. Yang, J. Yi, H. Zhang, Strengthening mechanism of cemented carbide containing Re, Mater. Sci. Eng. A 838 (2022) 142803, https://doi.org/10.1016/j.msea.2022.142803.
[10] I. Konyashin, S. Farag, B. Ries, B. Roebuck, WC-Co-Re cemented carbides: structure, properties and potential applications, Int. J. Refract. Met. Hard Mater. 78 (2019) 247–253, https://doi.org/10.1016/j.ijrmhm.2018.10.001.
[11] L.Y. Tian, R. Lizárraga, H. Larsson, E. Holmström, L. Vitos, A first principles study of the stacking fault energies for fcc Co-based binary alloys, Acta Mater. 136 (2017) 215–223, https://doi.org/10.1016/j.actamat.2017.07.010.
[12] X. Wu, N. Tao, Y. Hong, J. Lu, K. Lu, γ → ε martensite transformation and twinning deformation in fcc cobalt during surface mechanical attrition treatment, Scr. Mater. 52 (2005) 547–551, https://doi.org/10.1016/j.scriptamat.2004.12.004.
[13] P.A. Dubos, J. Fajoui, N. Iskounen, M. Coret, S. Kabra, J. Kelleher, B. Girault, D. Gloaguen, Temperature effect on strain-induced phase transformation of cobalt, Mater. Lett. 281 (2020) 128812, https://doi.org/10.1016/j.matlet.2020.128812.
[14] J. Tu, S. Zhang, Z. Zhou, H. Tang, Structural characterization of a special boundary between α plates after martensitic transformation in cobalt, Mater. Charact. 112 (2016) 219–223, https://doi.org/10.1016/j.matchar.2015.12.032.
[15] N. Haghdadi, P. Cizek, P.D. Hodgson, V. Tari, G.S. Rohrer, H. Beladi, Effect of ferrite-to-austenite phase transformation path on the interface crystallographic character distributions in a duplex stainless steel, Acta Mater. 145 (2018) 196–209, https://doi.org/10.1016/j.actamat.2017.11.057.
[16] H. Beladi, G.S. Rohrer, The role of thermomechanical routes on the distribution of grain boundary and interface plane orientations in transformed microstructures, Metall. Mater. Trans. A 48 (2017) 2781–2790, https://doi.org/10.1007/s11661-016-3630-4.

[17] P. Tolédano, G. Krexner, M. Prem, M. Prem, H.P. Weber, V.P. Dmitriev, Theory of the martensitic transformation in cobalt, Phys. Rev. B Condens. Matter Mater. Phys. 64 (2001) 144104, https://doi.org/10.1103/PhysRevB.64.144104.
[18] M. Eizadjou, H. Chen, C. Czettl, J. Pachlhofer, S. Primig, S.P. Ringer, An observation of the binder microstructure in WC-(Co+Ru) cemented carbides using transmission Kikuchi diffraction, Scr. Mater. 183 (2020) 55–60, https://doi.org/10.1016/j.scriptamat.2020.03.010.
[19] J.H. Yang, C.M. Wayman, On the secondary variants formed at intersections of ε martensite variants, Acta Metall. Mater. 40 (1992) 2011–2023, https://doi.org/10.1016/0956-7151(92)90187-J.
[20] J.H. Yang, C.M. Wayman, Intersecting-shear mechanisms for the formation of secondary ϵ martensite variants, Acta Metall. Mater. 40 (1992) 2025–2031, https://doi.org/10.1016/0956-7151(92)90188-K.
[21] R. Bauer, E.A. Jägle, W. Baumann, E.J. Mittemeijer, Kinetics of the allotropic hcp-fcc phase transformation in cobalt, Philos. Mag. 91 (2011) 437–457, https://doi.org/10.1080/14786435.2010.525541.
[22] C.C. Koch, C.J. McHargue, The influence of plastic deformation on the fccdhcp transformation in cerium, Acta Metall. 16 (1968) 1105–1115.
[23] M. Martinez, E. Hug, Characterization of deformation twinning in polycrystalline cobalt: a quantitative analysis, Materialia 7 (2019) 100420, https://doi.org/10.1016/j.mtla.2019.100420.
[24] K.P. Mingard, B. Roebuck, J. Marshall, G. Sweetman, Some aspects of the structure of cobalt and nickel binder phases in hardmetals, Acta Mater. 59 (2011) 2277–2290, https://doi.org/10.1016/j.actamat.2010.12.004.
[25] C. Cayron, Angular distortive matrices of phase transitions in the fcc-bcc-hcp system, Acta Mater. 111 (2016) 417–441, https://doi.org/10.1016/j.actamat.2016.01.075.
[26] K. Edalati, S. Toh, M. Arita, M. Watanabe, Z. Horita, High-pressure torsion of pure cobalt: hcp-fcc phase transformations and twinning during severe plastic deformation, Appl. Phys. Lett. 102 (2013) 181902, https://doi.org/10.1063/1.4804273.
[27] M. Martinez Celis, P. Minárik, E. Hug, J. Dorenlor, F. Chmelík, M. Knapek, P. Dobroň, Analysis of the twin variant selection in polycrystalline cobalt, J. Mater. Sci. 56 (2021) 7740–7752, https://doi.org/10.1007/s10853-020-05718-9.
[28] P. Xie, S. Shen, C. Wu, J. Chen, Abnormal orientation relation between fcc and hcp structures revealed in a deformed high manganese steel, J. Mater. Sci. Technol. 60 (2021) 156–161, https://doi.org/10.1016/j.jmst.2020.07.003.
[29] Q. Sun, X.Y. Zhang, R.S. Yin, Y. Ren, L. Tan, Structural characterization of {101-3} twin boundaries in deformed cobalt, Scr. Mater. 108 (2015) 109–112, https://doi.org/10.1016/j.scriptamat.2015.06.029.
[30] J. Hu, Y. Zhang, F. Han, W. Guo, M. Ali, J. Ren, Q. Wang, G. Li, Variants of face-centered cubic phase in pure hafnium during the HCP→FCC phase transformation, Mater. Charact. 206 (2023) 113451, https://doi.org/10.1016/j.matchar.2023.113451.
[31] D.M. Saylor, B.S. El-Dasher, B.L. Adams, G.S. Rohrer, Measuring the five-parameter grain-boundary distribution from observations of planar sections, Metall. Mater. Trans. A 35 (2004) 1981–1989, https://doi.org/10.1007/s11661-004-0147-z.
[32] H. Beladi, G.S. Rohrer, A.D. Rollett, V. Tari, P.D. Hodgson, The distribution of intervariant crystallographic planes in a lath martensite using five macroscopic parameters, Acta Mater. 63 (2014) 86–98, https://doi.org/10.1016/j.actamat.2013.10.010.
[33] N. Haghdadi, R. DeMott, P.L. Stephenson, X.Z. Liao, S.P. Ringer, S. Primig, Five-parameter characterization of intervariant boundaries in additively manufactured Ti-6Al-4V, Mater. Des. 196 (2020) 109177, https://doi.org/10.1016/j.matdes.2020.109177.
[34] E. Farabi, V. Tari, P.D. Hodgson, G.S. Rohrer, A.D. Rollett, H. Beladi, The role of thermomechanical processing routes on the grain boundary network of martensite in Ti–6Al–4V, Mater. Sci. Eng. A 822 (2021) 141665, https://doi.org/10.1016/j.msea.2021.141665.
[35] E. Farabi, V. Tari, P.D. Hodgson, G.S. Rohrer, H. Beladi, The role of phase transformation mechanism on the grain boundary network in a commercially pure titanium, Mater. Charact. 169 (2020) 110640, https://doi.org/10.1016/j.matchar.2020.110640.
[36] T. Waitz, H.P. Karnthaler, The f.c.c. to h.c.p. martensitic phase transformation in CoNi studied by TEM and AFM methods, Acta Mater. 45 (1997) 837–847, https://doi.org/10.1016/S1359-6454(96)00184-X.
[37] F. Berto, P. Lazzarin, Recent developments in brittle and quasi-brittle failure assessment of engineering materials by means of local approaches, Mater. Sci. Eng. R Rep. 75 (2014) 1–48, https://doi.org/10.1016/j.mser.2013.11.001.
[38] Y.T. Zhu, X.Y. Zhang, Q. Liu, Observation of twins in polycrystalline cobalt containing face-center-cubic and hexagonal-close-packed phases, Mater. Sci. Eng. A 528 (2011) 8145–8149, https://doi.org/10.1016/j.msea.2011.07.062.
[39] P. Asghari-Rad, M. Nili-Ahmadabadi, H. Shirazi, S. Hossein Nedjad, S. Koldorf, A significant improvement in the mechanical properties of AISI 304 stainless steel by a combined RCSR and annealing process, Adv. Eng. Mater. 19 (2017) 1600663, https://doi.org/10.1002/adem.201600663.
[40] M.X. Zhang, S.Q. Chen, H.P. Ren, P.M. Kelly, Crystallography of the simple HCP/FCC system, Metall. Mater. Trans. A (2008) 1077–1086, https://doi.org/10.1007/s11661-008-9497-2, 39 A.
[41] K. Glowinski, A. Morawiec, A toolbox for geometric grain boundary characterization, in: Proceedings of the 1st International Conference on 3D Materials Science, Springer, Cham, 2012, pp. 119–124.
[42] G.S. Rohrer, V. Randle, C. Kim, Changes in the five-parameter grain boundary character distribution in a -brass brought about by iterative thermomechanical processing, Acta Mater. 54 (2006) 4489–4502, https://doi.org/10.1016/j.actamat.2006.05.035.
[43] E. Farabi, P.D. Hodgson, G.S. Rohrer, H. Beladi, Five-parameter intervariant boundary characterization of martensite in commercially pure titanium, Acta Mater. 154 (2018) 147–160, https://doi.org/10.1016/j.actamat.2018.05.023.
[44] J. Gruber, D.C. George, A.P. Kuprat, G.S. Rohrer, A.D. Rollett, Effect of anisotropic grain boundary properties on grain boundary plane distributions during grain growth, Scr. Mater. 53 (2005) 351–355, https://doi.org/10.1016/j.scriptamat.2005.04.004.
[45] J. Gruber, H.M. Miller, T.D. Hoffmann, G.S. Rohrer, A.D. Rollett, Misorientation texture development during grain growth. Part I: simulation and experiment, Acta Mater. 57 (2009) 6102–6112, https://doi.org/10.1016/j.actamat.2009.08.036.
[46] S.J. Dillon, G.S. Rohrer, Mechanism for the development of anisotropic grain boundary character distributions during normal grain growth, Acta Mater. 57 (2009) 1–7, https://doi.org/10.1016/j.actamat.2008.08.062.
[47] A.P. Sutton, An analytic model for grain-boundary expansions and cleavage energies, Philos. Mag. A 63 (1991) 793–818, https://doi.org/10.1080/01418619108213914.
[48] Q. Fan, A new method of calculating interplanar spacing: the position-factor method, J. Appl. Crystallogr. 45 (2012) 1303–1308, https://doi.org/10.1107/S0021889812037764.
[49] V. Govindaraj, E. Farabi, S. Kada, P.D. Hodgson, R.P. Singh, G.S. Rohrer, H. Beladi, Effect of manganese on the grain boundary network of lath martensite in precipitation hardenable stainless steels, J. Alloys Compd. 886 (2021) 161333, https://doi.org/10.1016/j.jallcom.2021.161333.
[50] N. Haghdadi, P. Cizek, H. Beladi, P.D. Hodgson, A novel high-strain-rate ferrite dynamic softening mechanism facilitated by the interphase in the austenite/ferrite microstructure, Acta Mater. 126 (2017) 44–57, https://doi.org/10.1016/j.actamat.2016.12.045.
[51] E. Farabi, V. Tari, P.D. Hodgson, G.S. Rohrer, H. Beladi, On the grain boundary network characteristics in a martensitic Ti-6Al-4V alloy, J. Mater. Sci. 55 (2020) 15299–15321, https://doi.org/10.1007/s10853-020-05075-7.
[52] A.H. Barry, G. Dirras, F. Schoenstein, F. Tétard, N. Jouini, Microstructure and mechanical properties of bulk highly faulted fcc/hcp nanostructured cobalt microstructures, Mater. Charact. 91 (2014) 26–33, https://doi.org/10.1016/j.matchar.2014.02.004.